ADVANCED FUNCTIONAL MATERIALS
www.afm-journal.de

Distributed Feedback Lasers Based on Thiophene/Phenylene Co-Oligomer Single Crystals

Hong-Hua Fang, Ran Ding, Shi-Yang Lu, Jie Yang, Xu-Lin Zhang, Rui Yang, Jing Feng, Qi-Dai Chen, Jun-Feng Song, and Hong-Bo Sun**

Organic crystals have great potential for the applications in laser devices. This article presents an effective approach for fabrication of distributed feedback single crystal lasers. With the laser interference ablation method, high quality grating structures have been fabricated on the organic single-crystalline thin film materials. The relationship between the depth, periodicity, and laser fluence is discussed. The optical properties, such as photoluminescence, and diffractive properties are studied in detail. With the appropriate period, strong laser emission has been observed from these devices. Distributed feedback lasing is demonstrated from the laser interference ablated organic single crystals for the first time.

1. Introduction

Organic solid state lasers have attracted considerable attentions because they have the potential to be tunable, flexible, biocompatible, and easily integrated into plastic optoelectronics.[1–8] Optically pumped laser has been reported in a very broad range of conjugated polymers and oligomers. However, for the electrically pumped organic lasers, there still exist many challenging problems to be resolved.[5,9–11] One is that the organic devices have been damaged before the injected current reaches the expected threshold current density (kA/cm^2 range) for electrically driven lasing due to the low charge carrier mobilities of the disordered amorphous materials. In the view of carrier transport and charge injection, single crystalline organic semiconductors are recognized as potential building blocks for electrically pumped organic lasers. The long-range order and high chemical purity in crystals make them intrinsically excellent in charge-carrier transport properties, whose mobility could be significantly increased by three orders or more from their amorphous phase to the single-crystal phase without any serious luminescence efficiency decrease.[12–15] Notable achievements on the amplified spontaneous emission (ASE) have been attained in a large number of crystalline materials.[16–22] For a laser device, resonator structure is necessary to apply the positive optical feedback, which may reduce the lasing threshold significantly. Within this framework, several attempts were made to construct a resonator for crystals. Examples include the use of naturally formed cleaved facet as Fabry-Pérot resonator,[23–24] or the microcavities fabricated with electron-beam (EB) lithography and reactive ion etching.[25–27] With the help of these resonators, the lasing threshold could be reduced to half or a fifth of the values observed for the bulk crystals.

As counterpart of cavity resonators, diffractive resonators, such as distributed feedback (DFB),[28–32] are extensively investigated. They can be readily incorporated into planar organic semiconductor waveguides and allow surface emission. These kinds of resonators have witnessed the great success in the polymer materials. A variety of fabrication schemes have been demonstrated to construct the DFB cavities, such as UV embossing, nanoimprint lithography, soft lithography, liquid imprinting, micromolding. Unfortunately, most of these methods are limited to organic crystals, because they are generally sensitive to solvent and the fragility makes them difficult to handle. As a dry method, laser ablation has been reported to process the organic materials. Although it has been used to fabricate polymer/amorphous organic DFB lasers,[32–33] organic crystal DFB laser has not been reported, as far as we know.

In this work, we have achieved distributed feedback laser based on the organic single-crystalline thin film materials. Diffractive resonators in the high-quality thin film crystals could be easily fabricated with a one-step, noncontact, and dry method – ultraviolet (UV) laser interference ablation (LIA). Different periodic gratings with optical quality could be directly formed in the crystals by changing the incident angle of the interference beam. With the help of the right periodic structures, distributed feedback (DFB) resonators were constructed in the crystals to provide the feedback. In particular, we observed laser emission with threshold of E_{th} = 25 μJ cm^{-2} in the distributed feedback resonators. More important, this method avoids both the dissolution of organic crystals and the need of good-quality end facets. This is a crucial aspect for future implementations of high-yield production.

H.-H. Fang, R. Ding, S.-Y. Lu, J. Yang, X.-L. Zhang, R. Yang, Prof. J. Feng, Dr. Q.-D. Chen, Prof. J.-F. Song, Prof. H.-B. Sun
State Key Laboratory on Integrated Optoelectronics
College of Electronic Science and Engineering
Jilin University
2699 Qianjin Street, Changchun, 130012, China
E-mail: jingfeng@jlu.edu.cn; hbsun@jlu.edu.cn
S.-Y. Lu, Prof. H.-B. Sun
College of Physics
Jilin University
119 Jiefang Road, Changchun, 130023, China

DOI: 10.1002/adfm.201101467

2. Experimental Design

Figure 1 shows the experimental setup for the fabricating the DFB structures. Firstly, UV-curable adhesive NOA61 resist was spin-coated to form about 100 nm thickness film on the cleaned substrate. Then, the grown crystal plates were transferred from the quartz tube onto the substrate. The crystals were then adhered onto the substrate under the UV irradiation. After that, the prepared samples were exposed to the interference pattern of high power laser and their surfaces were structured by two-beam laser interference patterning to achieve line-like patterns on the surface. Their depth and periodicity are controlled by the laser fluence and the angle between the interfering laser beams. Under the UV excitation, the fluorescence from the crystals is waveguided in the higher refractive index organic thin film crystals and gets scattered by the periodic corrugations. If the period of the corrugations is suitable, the scattered light from each corrugation can combine through constructive interference to create a "Bragg scattered" wave that also propagates within the film but in a different direction. The DFB lasing occurs when the wavelength λ of the light satisfies the Bragg expression,[4]

$$2n_{\mathrm{eff}}\Lambda = m\lambda \quad (1)$$

where Λ is the periodicity of the grating, m is the order bragg refection, and n_{eff} is the effective refractive index of the waveguide, which is a geometrical average of the refractive indices of the layers of the waveguide and can be calculated through a solution of the Helmholtz wave equation for a planar multilayer structure.

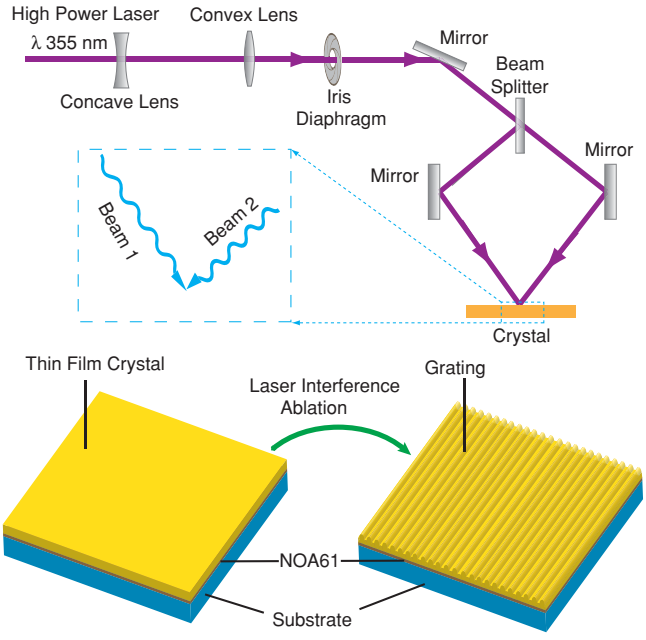

Figure 1. Schematics of experimental setup for the laser interference ablation (LIA). A 10 ns pulsed Nd:YAG laser (Quanta-Ray, Spectra Physics) with wavelength of 355 nm is used as the laser source. The primary laser beam was split into two coherent light beams (beams 1 and 2). The interference between beam 1 and 2 formed a grating pattern on the crystal surface. The main fabrication process for the crystals include: growth of thin film single crystal, transfer the crystals onto the substrate, LIA.

3. Results and Discussion

3.1. The Characteristic of Grown Thin-Film Crystals

Amongst organic molecular semiconductors thiophene/phenylene co-oligomers are counted as promising materials because of their unique optoelectronic properties.[14,34–36] Herein, crystals of a high hole mobility (0.66 $cm^2\ V^{-1}\ s^{-1}$) co-oligomers,[37] 2,2′-bithiophene,5,5′-bis([1,1′-biphenyl]-4-yl) (BP2T, see its structural formula in inset of **Figure 2**a) was used. The single crystals were grown by physical vapor transport in a flowing stream of argon (Figure S1 in the Supporting Information). This enabled the BP2T single crystals to grow as large as 5 mm × 5 mm with thickness varying from 200 nm to 10 µm. Figure 2a shows the photograph of a typical thin plate crystal under the daylight. The smooth surface morphology shown in the scanning electron microscopy (SEM) image (Figure 2c) suggests the high quality of grown crystals. The slab planes exhibit molecular-scale flatness with steps of about 2.58 nm (approximately 1 step per 2–5 µm), as confirmed by atomic force microscope (AFM) observations presented in Figure 2d. This step size is about half the lattice constant (Figure 2e) of 5.3 nm for *c*-axis of a BP2T crystal (i.e., the length of a single molecule). In the crystals of BP2T, molecules stand nearly perpendicular to the bottom crystal plane (i.e., the *ab*-plane), which was confirmed by the X-ray diffraction pattern (Figure S2 in the Supporting Information). According to the Bragg equation we can calculate that the thickness of one BP2T molecular layer is 2.54 nm, which corresponds to the height of one step in the AFM image. The emissions in the crystals, therefore, tend to be propagated as a waveguide mode along the slab crystal plane. As shown in the Figure 2b, orange fluorescence emitted only from the edges of the crystal without any emission from inside at all. This shows that the excellence of the waveguide properties of BP2T crystals. If the effective refractive index of the slab crystal is periodically modulated, both distributed feedback and output coupling of the waveguide mode could be supported by Bragg scattering, then distributed feedback lasing may occur from these structured crystals.

3.2. Fabrication of Grating on the Crystals

For the fabrication of grating on the crystal surface, the primary laser beam (355 nm) was split into two coherent light beams. Interference between the beams formed a grating pattern (Figure 1) on the crystal surface. The period (d) of the grating pattern is determined by the wavelength (λ) of the light and the half angle (θ) between the two incident beams through the relationship $d = \lambda/2\sin(\theta)$. During laser interference patterning, the high-energy nanosecond laser selectively ablates the crystal surface. The crystal located at the bright fringes of the interference pattern is "vaporized" and removed, while the materials at the dark fringes remains unchanged, forming the grating structures on the crystal surface. **Figure 3**a, b shows the scanning electron microscopy (SEM) images of cross section of an ablated crystal after direct laser interference ablation. The surface ablation depth (Δh) was approximately 230 nm, that is,

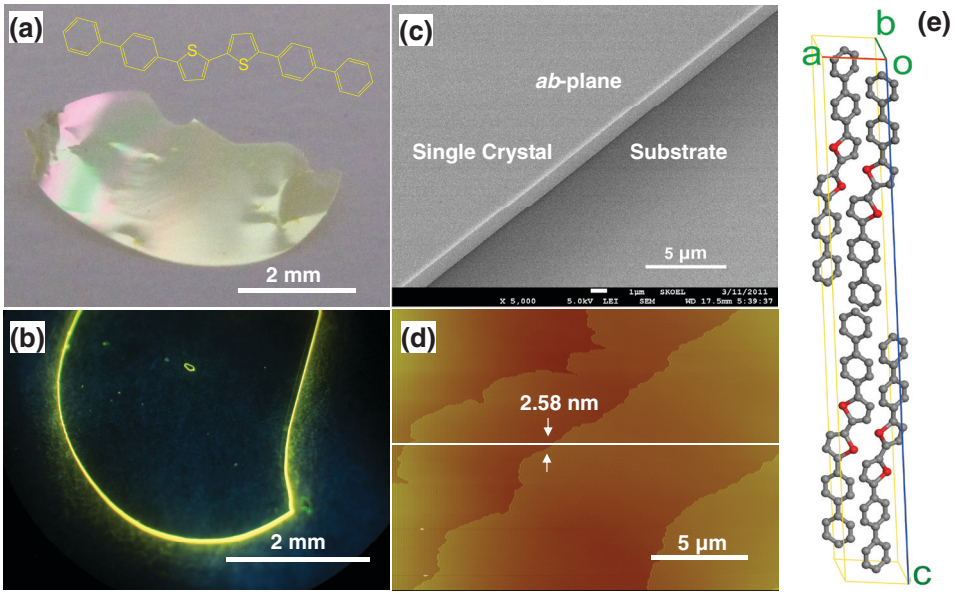

Figure 2. a) Global view of a BP2T single crystal under the daylight. Inset: chemical structure of BP2T. b) Fluorescence photograph of BP2T crystal under the UV light irradiation. c) Scanning electron microscope image of BP2T crystal. The ab-plane parallels the substrate plane. d) The surface profile investigated by the AFM; and their cross-section analyses. e) Crystal packing of BP2T.

much deeper than that of conventional DFB gratings fabricated on the polymers.

Experiments show that the pulse energy must exceed a certain threshold to achieve the removal of the materials at the bright interference fringes. Variations of the laser-beam intensity and processing time will result in change of the duty circle and depth of the gratings (Figure S3 in Supporting Information). Figure 3c shows an AFM image of the grating structure (period of about 800 nm). The modulation depth is deeper than 200 nm. The modulation depth could be controlled by adjusting the laser-beam intensity. Figure 3d shows the ablation depth as a function of the laser fluence. Each data point was obtained by averaging the ablation depth over the whole measurement area (5 μm × 5 μm). The insets show three profiles of the patterned BP2T crystal, which can be found that the higher the laser fluence, the smaller the width, as well as the depth. It should be noted that the ablation threshold is dependent on the crystallographic orientation. For example, the threshold is below 0.26 W/cm^2 when grating vector is parallel to the a-axis, while the threshold is much higher than this value. By controlling the laser fluence and processing time, well structured gratings can be produced.

3.3. Optical Properties of Crystal Gratings

In order to study the ablation effect on the optical properties of the crystals, the absorption spectra and photoluminescence quantum yield (QY) the crystals before and after ablation processes were comparably investigated. The results of the absorbance measurements are presented in the Supporting Information, Figure S6. Using fluence 0.3 W/cm^2, no significant absorption changes are detected. The QY for the ablated and unablated crystals, determined with an integrating sphere, are 55% and 59%, respectively. Considering the measurement error, it shows that no evident decrease in QY during the ablation process. Thus we conclude that the optical properties of the crystal are not significantly harmed by the ablation process. **Figure 4**a shows the spectrum detected at normal to the waveguide plane of the crystal with and without the fabricated gratings. It is clear that the presence of the grating structure drastically modifies the spontaneous emission. Bragg-scattered spontaneous emission from the BP2T crystal waveguide appears as two relatively narrow features in the output spectrum below threshold when collecting light scattered at the angle of normal incidence. The dip corresponds to the optical stop band of the one dimensional grating.

A He-Ne laser (633 nm) was employed to irradiate the grating (period 800 nm, depth 200nm). Its wavelength does not exhibit any absorption. The incident angle of the beam was adjusted to have the maximum intensity of the first diffracted line. Figure 4b present the diffraction pattern when illuminated under the He–Ne laser. Two diffraction orders (0 and ±1) can be clearly seen on the screen. The zero-order transmitted (I_0) and the first-order diffracted (I_1) lines of the reading beam, were used for the calculation of the diffraction efficiency (DE), DE = I_1/I_0. The sinusoidal phase grating model was adopted for the theoretical diffraction efficiency analysis.[38] The experimental DE is about 27%, which is about 80% of that of theory value (33.8%). Under the white illumination, we can see the white spot in the centre of the screen which corresponds to image of the grating in zero order of spectrum (Figure 4c). Diffracted color patterns are formed on the left and right, corresponding to a spectral composition of the light. These excellent diffraction properties demonstrates the optical-quality of the fabricated gratings, showing great potential for high quality DFB lasers.

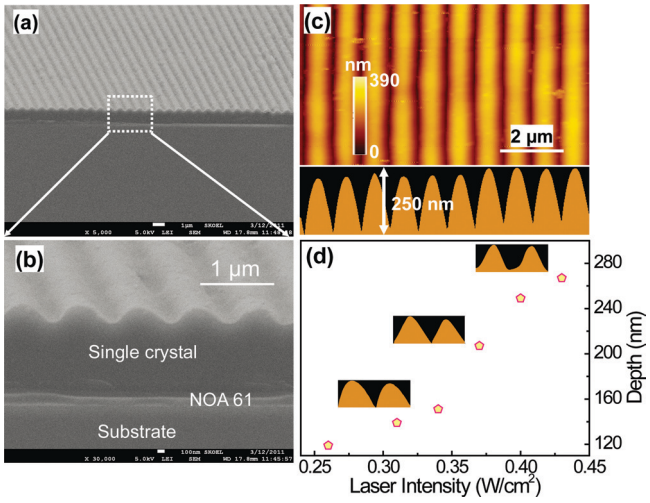

Figure 3. a) Image of thin film crystals fabricated with 800 nm period grating. b) Enlarged SEM image of side view. c) AFM images for the topographies of laser interference ablation of BP2T crystals with laser fluences 0.4 Wcm^{-2}. d) The ablation depth as a function of laser fluence. The insets are AFM profile images for representative data points.

3.4. Lasing Performance

The device (crystal thickness 1 μm, modulation depth 115 nm, period 640 nm) was excited by the 400 nm femtosecond pump beam and the emission was collected by an optical fiber connected to a spectrograph (**Figure 5**a). The emission spectra were then recorded as a function of increasing pump power. As the excitation pump energy is increased above a critical threshold, strong yellow–green emission consisting of two arc lines can be observed. Figure 5b shows photographs of one of the arc lines emitted from the device, which is at an angle of 30° normal to the plane of the crystal. Most of the laser energy is focused in the center area of the spot. The wavelength emission is centered at 565 nm with full width at half maximum (FWHM) of ~1.5 nm (**Figure 6**a). PL intensity of emission of a device as a function of the incident laser energy intensity is shown in Figure 6b. The threshold is determined to 25 $\mu J/cm^2$, which is 3 times lower than that (~75 $\mu J/cm^2$) of unablated crystal, and more lower that the uniformly ablated crystal (described in the Supporting Information, Figure S7).

To further confirm that it is DFB lasing, we have calculated the Bragg diffraction wavelength λ_{Bragg}. The refractive indices of BP2T thin crystals are estimated on the basis of both the thin-film interference in the reflectance spectrum and crystal thickness (details can be found in Figure S4 and S5, Supporting Information). The calculation of n_{eff} is based on three-layer planar waveguide model, in which $n_{crystal}$ = 1.80, n_{NOA61} = 1.56, n_{quartz} = 1.46, n_{air} = 1. We obtain n_{eff} = 1.73 at 565 nm for TE_1 mode and the m = 4. This was in good agreement with the observed lasing wavelength, considering measurement error of the refractive indices and the thickness of the crystal layer.

The lasing wave are simultaneously diffracted by the grating, where the outcoupled angle of lasing wavelength is defined:

$$n_{eff}\Lambda(\sin\alpha + \sin\theta) = l\lambda / = 0, 1, 2 \quad (2)$$

Combination of Equation (1) and (2) yields an expression for θ:[39]

$$\sin\theta = \frac{2l}{m} - 1,\ \theta \in \left[-\frac{\pi}{2}, \frac{\pi}{2}\right] \quad (3)$$

Here, l is the diffracted order and m is the order bragg refection. The observed emissions in the Figure 5b (at an angle of 30° normal to the plane of the waveguide) is consistent with the lasing beam l = 1 or 3.

4. Conclusions

In summary, we have fabricated high quality distributed feedback resonators in organic single-crystalline thin film materials for the first time. Strong lasing emissions have been observed

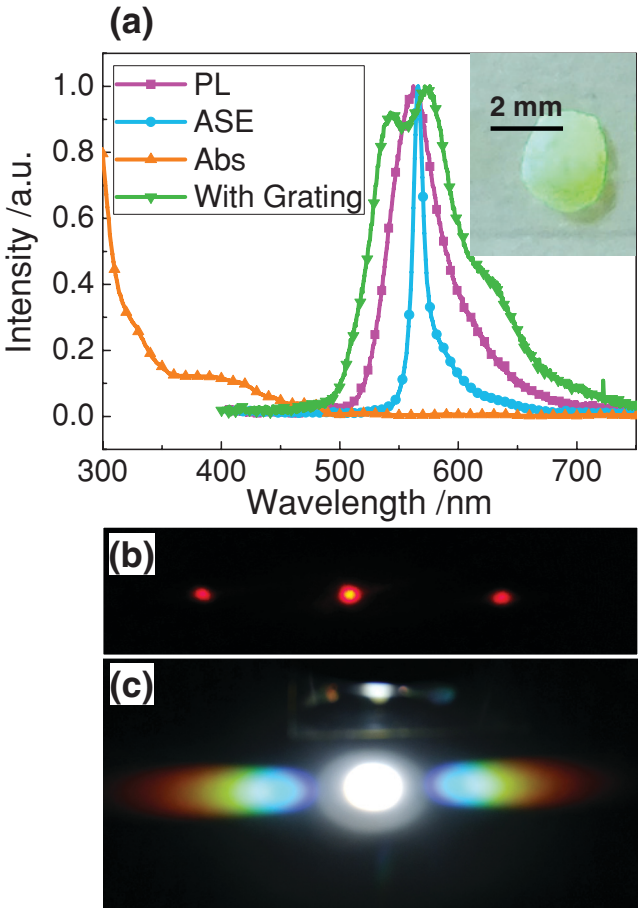

Figure 4. a) The absorption (Abs), photoluminescence spectra (PL), Bragg-scattered spontaneous emission (with grating) and amplified spontaneous emission (ASE) spectra of BP2T crystals. The photoluminescence spectra and the Bragg-scattered spontaneous emission are detected at an angle normal to the plane of crystals. The FWHM for ASE spectrum is 9 nm. Inset: Iridescence color caused by the diffraction of the fabricated grating (800 nm period) in the crystal. Diffraction patterns of the prepared grating (800 nm period) irradiated by He-Ne laser beam (b) and white light (c).

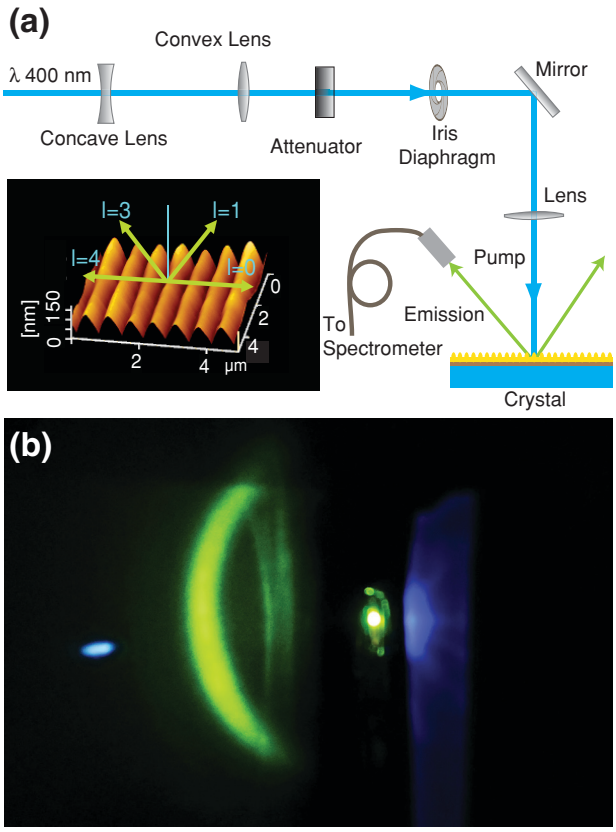

Figure 5. a) Experimental setup used for characterization of organic single crystal lasers. Inset: AFM images of the DFB and the sketch of directions of out-of-plane scattering for DFB structures of m = 4. b) Photographs of the operating single crystal laser based on 1D DFB structure.

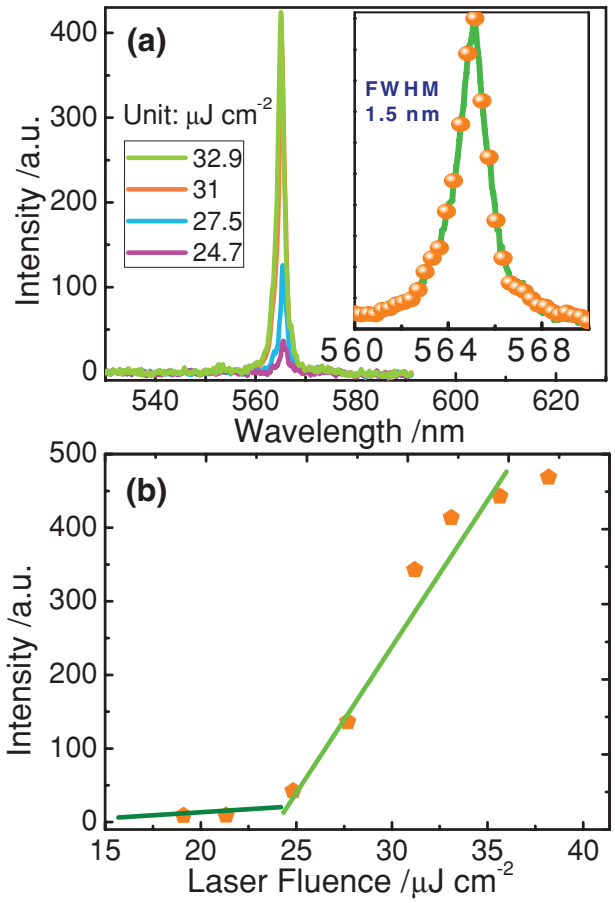

Figure 6. a) Measured spectra of the lasing emission of the laser at different pump fluence, showing a center wavelength of about 565 nm and a linewidth of about 1.5 nm. b) Output intensity as a function of the pump fluence, indicating a pump threshold of about 25 μJ cm^{-2}.

from these devices. The lasing threshold in DFB resonators is reduced by a factor of 3 in comparison with the ASE threshold value of the BP2T film. The laser interference ablation method proved a dry, low-cost and single-step technique, consisting of short-time exposure of high power laser, enables mass fabrication of high quality single-crystal lasers based on DFB mechanisms for active photonic devices. The combination of high gain and high mobility organic crystals with laser interference ablation techniques is a promising approach to organic semiconductor lasers.

5. Experimental Section

Crystal Growth and Preparation: The materials of BP2T were purchased from Lumtec Corp., and was used without further purified. The single crystals were grown in a horizontal physical vapor transport apparatus. A quartz boat loaded with the BP2T powder was put into the center of a quartz tube, which was inserted into the high temperature zone of the tube furnace. An initial sublimation temperature at about 380 °C was employed, while deposition temperature was set at 340 °C. High-purity nitrogen was adopted as carrier and to prevent the organic materials from being oxidized, and the gas flowing rate was kept at 100 mL/min. The grown single crystals were hanged inside the growth tubes, and could be taken out with tweezers easily. Then the high quality crystals were chosen and adhered onto the substrate on which there is a layer of UV-curable adhesive NOA61 resist (~100 nm thickness).

Laser Inference Ablation: In the experiment, A Nd-YAG nanosecond-pulsed laser (Quanta-Ray Lab, Spectra Physics) was employed as the coherent light source for the interference ablation. 355 nm radiations were used, which is the third harmonic of its fundamental wavelength (1064 nm). The laser power could be adjusted through the controller of the laser and is monitored by a high damage threshold power meter. An electromechanical shutter controls the exposure time. The samples were loaded on the stage and exposed to the pulsed interference pattern. All the experiments are performed in an ambient atmosphere environment. A beam expander was used in the experiment so as to achieve uniform fluence in the central patterned area.

Lasing Characteristics: The second harmonic generation (400nm) of a regenerative amplifier (Spitfire, Spectra Physics) was used as the pump source. The spot size of the pump laser on the samples was estimated to be about 1 mm in radius. The pump pulse energy is controlled by sending the laser beam through an attenuator wheel. The emitted light was detected by the optical fiber and then dispersed to the spectrometer connected with CCD.

Instrumentation: SEM images were obtained from a Jeol-7500F microscope. Samples were coated with approximately 5–10 nm of gold before imaging. The film thicknesses for BP2T crystals were measured using a profilometer (Dektak 150), atomic force microscope (Nanoscope IIIa scanning probe microscope and Nanonavi), and the previously described SEM instrument. X-ray diffraction was carried out on a Rigaku R-AXIS RAPID diffractometer (D/max-rA, using Cu Kα radiation of wavelength 1.542 Å). Optical absorption data were

collected with a Shimadzu UV-3600 spectrophotometer equipped with an integrating sphere (in order to eliminate the scattering effect). The photoluminescence quantum yields of the crystals were measured in an integrated sphere.

Supporting Information

Supporting Information is available from the Wiley Online Library or from the author.

Acknowledgements

The authors gratefully acknowledge the supports from National Basic Research Program of China (973 Program) under Grant No. 201tel1CB013005, and from Natural Science Foundation of China (NSFC) under grants Nos. 90923037 and 61177024. Hong-Hua Fang acknowledge the supports from Graduate Interdisciplinary Fund of Jilin University (No. 2011J008)

Received: June 30, 2011
Published online: October 6, 2011

[1] F. Hide, M. A. Diaz-Garcia, B. J. Schwartz, M. R. Andersson, Q. Pei, A. J. Heeger, *Science* **1996**, *273*, 1833.
[2] N. Tessler, *Adv. Mater.* **1999**, *11*, 363.
[3] M. D. McGehee, A. J. Heeger, *Adv. Mater.* **2000**, *12*, 1655.
[4] I. D. W. Samuel, G. A. Turnbull, *Chem. Rev.* **2007**, *107*, 1272.
[5] J. Clark, G. Lanzani, *Nat. Photonics* **2010**, *4*, 438.
[6] H. Coles, S. Morris, *Nat. Photonics* **2010**, *4*, 676.
[7] S. Kena-Cohen, S. R. Forrest, *Nat. Photonics* **2010**, *4*, 371.
[8] H. H. Fang, B. Xu, Q. D. Chen, R. Ding, F. P. Chen, J. Yang, R. Wang, W. J. Tian, J. Feng, H. Y. Wang, H. B. Sun, *IEEE J. Quantum Electron.* **2010**, *46*, 1175.
[9] B. K. Yap, R. D. Xia, M. Campoy-Quiles, P. N. Stavrinou, D. D. C. Bradley, *Nat. Mater.* **2008**, *7*, 376.
[10] I. D. W. Samuel, E. B. Namdas, G. A. Turnbull, *Nat. Photonics* **2009**, *3*, 546.
[11] H. Kim, N. Schulte, G. Zhou, K. Mullen, F. Laquai, *Adv. Mater.* **2011**, *23*, 894.
[12] T. Oyamada, H. Uchiuzou, S. Akiyama, Y. Oku, N. Shimoji, K. Matsushige, H. Sasabe, C. Adachi, *J. Appl. Phys.* **2005**, *98*, 074506.
[13] T. Takenobu, S. Z. Bisri, T. Takahashi, M. Yahiro, C. Adachi, Y. Iwasa, *Phys. Rev. Lett.* **2008**, *100*, 066601.
[14] S. Z. Bisri, T. Takenobu, Y. Yomogida, H. Shimotani, T. Yamao, S. Hotta, Y. Iwasa, *Adv. Funct. Mater.* **2009**, *19*, 1728.
[15] K. Sawabe, T. Takenobu, S. Z. Bisri, T. Yamao, S. Hotta, Y. Iwasa, *Appl. Phys. Lett.* **2010**, *97*, 043307.
[16] H. Yanagi, T. Ohara, T. Morikawa, *Adv. Mater.* **2001**, *13*, 1452.
[17] M. Ichikawa, R. Hibino, M. Inoue, T. Haritani, S. Hotta, T. Koyama, Y. Taniguchi, *Adv. Mater.* **2003**, *15*, 213.
[18] W. J. Xie, Y. P. Li, F. Li, F. Z. Shen, Y. G. Ma, *Appl. Phys. Lett.* **2007**, *90*, 141110.
[19] R. Kabe, H. Nakanotani, T. Sakanoue, M. Yahiro, C. Adachi, *Adv. Mater.* **2009**, *21*, 4034.
[20] H. H. Fang, Q. D. Chen, R. Ding, J. Yang, Y. G. Ma, H. Y. Wang, B. R. Gao, J. Feng, H. B. Sun, *Opt. Lett.* **2010**, *35*, 2561.
[21] H. H. Fang, Q. D. Chen, J. Yang, H. Xia, B. R. Gao, J. Feng, Y. G. Ma, H. B. Sun, *J. Phys. Chem. C* **2010**, *114*, 11958.
[22] H. H. Fang, Q. D. Chen, J. Yang, H. Xia, Y. G. Ma, H. Y. Wang, H. B. Sun, *Opt. Lett.* **2010**, *35*, 441.
[23] M. Ichikawa, R. Hibino, M. Inoue, T. Haritani, S. Hotta, K. Araki, T. Koyama, Y. Taniguchi, *Adv. Mater.* **2005**, *17*, 2073.
[24] T. Yamao, K. Yamamoto, Y. Taniguchi, T. Miki, S. Hotta, *J. Appl. Phys.* **2008**, *103*, 093115.
[25] F. Sasaki, S. Kobayashi, S. Haraichi, S. Fujiwara, K. Bando, Y. Masumoto, S. Hotta, *Adv. Mater.* **2007**, *19*, 3653.
[26] S. Fujiwara, K. Bando, Y. Masumoto, F. Sasaki, S. Kobayashi, S. Haraichi, S. Hotta, *Appl. Phys. Lett.* **2007**, *91*, 021104.
[27] F. Sasaki, M. Mori, S. Haraichi, Y. Ido, Y. Masumoto, S. Hotta, *Org. Electron.* **2010**, *11*, 1192.
[28] J. R. Lawrence, G. A. Turnbull, I. D. W. Samuel, *Appl. Phys. Lett.* **2003**, *82*, 4023.
[29] D. A. Acevedo, A. F. Lasagni, C. A. Barbero, F. Mucklich, *Adv. Mater.* **2007**, *19*, 1272.
[30] E. B. Namdas, M. Tong, P. Ledochowitsch, S. R. Mednick, J. D. Yuen, D. Moses, A. J. Heeger, *Adv. Mater.* **2009**, *21*, 799.
[31] W. Y. Lai, R. D. Xia, Q. Y. He, P. A. Levermore, W. Huang, D. D. C. Bradley, *Adv. Mater.* **2009**, *21*, 355.
[32] T. Zhai, X. Zhang, Z. Pang, F. Dou, *Adv. Mater.* **2010**, *23*, 1860.
[33] M. Stroisch, T. Woggon, U. Lemmer, G. Bastian, G. Violakis, S. Pissadakis, *Opt. Express* **2007**, *15*, 3968.
[34] R. Hibino, M. Nagawa, S. Hotta, M. Ichikawa, T. Koyama, Y. Taniguchi, *Adv. Mater.* **2002**, *14*, 119.
[35] S. Hotta, M. Goto, R. Azumi, M. Inoue, M. Ichikawa, Y. Taniguchi, *Chem. Mater.* **2004**, *16*, 237.
[36] T. Yamao, Y. Sakurai, K. Terasaki, Y. Shimizu, H. Jinnai, S. Hotta, *Adv. Mater.* **2010**, *22*, 3078.
[37] M. Ichikawa, H. Yanagi, Y. Shimizu, S. Hotta, N. Suganuma, T. Koyama, Y. Taniguchi, *Adv. Mater.* **2002**, *14*, 1272.
[38] J. W. Goodman, *Introduction to Fourier optics*, Roberts & Company Publishers, Greenwood Village, USA **2005**.
[39] *Integrated Optics: Theory and Technology*, 5th edition, Springer-Verlag: Berlin Haeidelberg, **2002**.